possibility of retinal damage by surgery cannot be excluded [2, 5]. On the other hand, the STS prosthesis is inserted into a scleral pocket [8] or suprachoroidal space [7, 9], and the electrodes are not in direct contact with the retina, so only minimal surgical damage to the retina can occur [6, 11].

When using our STS-type retinal prosthesis, current pulses of up to 0.5 μC/phase must be delivered safely [11]. This exceeds the charge delivery capacity of conventional planar platinum electrodes [12]. To obtain a 0.5-μC/phase charge injection, we previously proposed a 0.5-mm-high bullet-shaped electrode using bulk micromachining [13]. However, in a few cases of chronic implantation in rabbits, retinal damage due to mechanical pressure from the electrode was observed (data not shown). To decrease mechanical pressure to the retina by lowering the electrode height, we developed a technique for increasing the surface area through electrochemical etching [14]. Increasing the surface area enabled a 40 % reduction in electrode height because of the high charge injection capacity. This new electrode was 0.3 mm in height [14]. However, the electrochemically treated electrode has not been evaluated for its effectiveness in stimulating retinal neurons.

The effects of using multiple electrodes for stimulating the retina have been evaluated in vitro using microfabricated multielectrode arrays [15] or by electrophysiologic methods on the visual cortex [16, 17]. However, it had been difficult to evaluate the resolving power of the retinal prosthesis in situ. We showed that functional imaging of the intrinsic retinal signal can be effective for evaluating the area stimulated by an STS prosthesis [18]. In that study, we used a single platinum electrode attached to the sclera.

The purpose of the study reported here was to evaluate electrochemically treated multiple platinum electrodes in stimulating the retina when implanted in a scleral pocket. We used retinal functional imaging not only to determine whether the retina was activated but also to determine the effect of STS array placement in the sclera pocket on the activation threshold.

Materials and methods

Cats

Seven eyes of seven cats (both sexes; weight 3–4 kg) were used for these experiments. All experiments were performed in accordance with the Association for Research in Vision and Ophthalmology (ARVO) Statement for the Use of Animals in Ophthalmic and Visual Research, and the procedures were approved by the Animal Research Committee of the Osaka University Medical School.

General preparation

The cats were initially given an intramuscular injection of ketamine hydrochloride (25 mg/kg) and an intraperitoneal injection of atropine sulfate (0.1 mg/kg). Each animal was anesthetized with an intravenous infusion of pentobarbital sodium (1 mg/kg/h) and paralyzed with pancuronium bromide (0.2 mg/kg/h) mixed with Ringer's solution and glucose (0.1 g/kg/h). Each cat was artificially ventilated with a mixture of nitrous oxide/oxygen (N_2O/O_2) (1:1); end-tidal carbon dioxide (CO_2) concentration was controlled at 4.0–5.5 % by altering ventilation frequency and volume. In addition to continuous monitoring of the expired CO_2, intratracheal pressure and electrocardiogram were also monitored. The body temperature was maintained with a heating pad at 38 °C. The pupils were dilated with 1 % atropine sulfate (Nihon Tenganyaku Institute, Nagoya, Japan) and 5 % phenylephrine hydrochloride (Kowa Company, Nagoya, Japan).

Optical imaging of the retina

The ocular fundus was monitored using a fundus camera (TRC-50LX; Topcon Corporation, Tokyo, Japan) with a digital CCD camera (C8484; Hamamatsu Photonics, Hamamatsu, Japan). The camera has a resolution of 1,280 × 1,024 pixels; however, the binning mode was used to obtain maximum light sensitivity, and the resolution was reduced to 320 × 256 pixels. To evaluate reflectance, a 12-bit digitizer was used, and a grayscale value (GSV) of 4,096 was obtained for each pixel. A halogen lamp was used to illuminate the posterior fundus, and a band-pass filter was inserted in the optical path to limit the wavelength passing to the fundus to between 800 and 880 nm. All experiments were performed in a dark room after 30 min of dark adaptation.

During each experiment, gray-scale images of the fundus were continually recorded at intervals of 25 ms for 25 s between 2 s before and 20 s after electrical stimulation. Trials were repeated ten times in each session. To improve the signal-to-noise ratio (SNR), images in all trials were averaged for each time point from the onset of the electrical stimulation. In addition, ten serial images were averaged every 250 ms. A 2D map of reflectance changes was obtained by subtracting raw fundus images taken before from those taken after stimulation.

Electrophysiologic recording from the optic chiasm

To record responses of retinal ganglion cells elicited by the electrical stimulation, bipolar stainless-steel electrodes were stereotaxically placed in the optic chiasm. The electrode was inserted from the cortical surface 13–14 mm

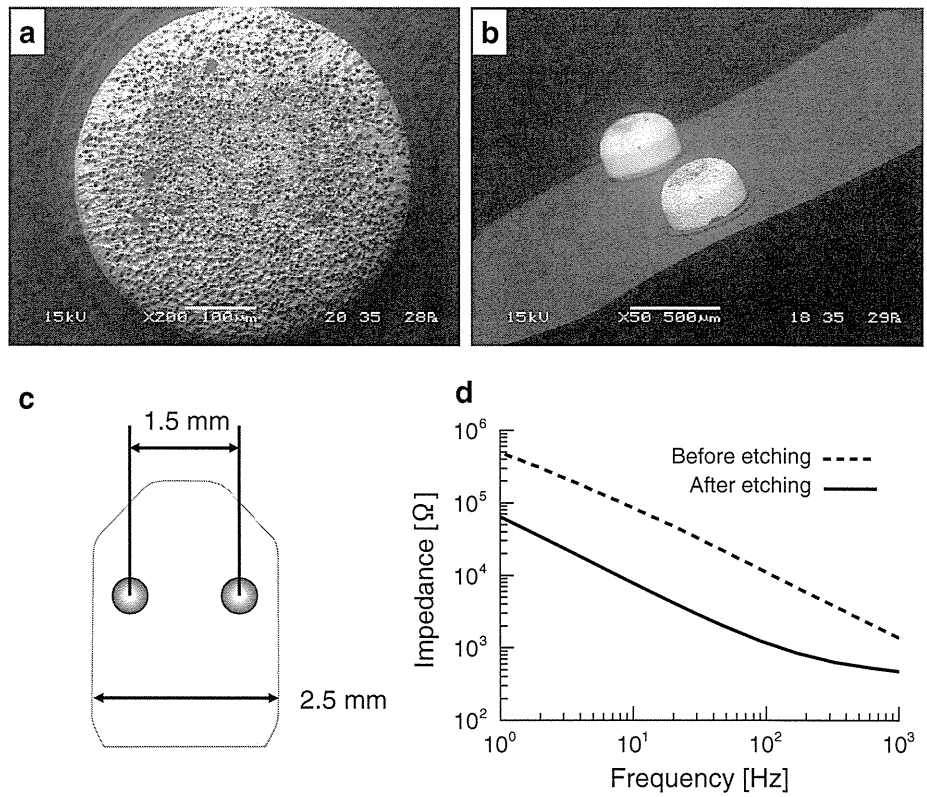

Fig. 1 Electrochemical treatment to platinum bulk electrode. **a** Scanning electron microscopic (SEM) image of the pitted electrode. A high density of pits can be seen on the surface of the bullet-shaped electrode, which increased the surface area. The pores were made by electrochemical etching. **b** SEM image of the stimulating electrode array. **c** SEM array consists of two porous electrodes with a center-to-center distance of 1.5 mm. **d** Frequency dependence of electrode impedance. The *dashed line* indicates impedance of the electrode before etching. The *solid line* indicates impedance of the electrode after etching

anterior to the ear bar and 1–2 mm ipsilateral to the midline. The depth of the electrode tip was 23–26 mm from the cortical surface. The flash-evoked response from the electrode was monitored to determine whether the electrode was in the optic chiasm. The recorded signal from the bipolar electrode was amplified 5,000 times and band-pass filtered from 10 Hz to 5 kHz using an AC-amplifier (Model 1800 Microelectrode AC amplifier; A-M SYSTEMS, Sequim, WA, USA) and a signal conditioner (LPF-202A; Warner Instruments, Hamden, CT, USA). The amplified signal was recorded with a signal processor (Power 1401; Cambridge Electronic Design, Cambridge, UK) with a sampling frequency of 50 kHz and analyzed offline with Signal 4 software (Cambridge Electronic Design). The signal was also monitored on an oscilloscope and an audio monitor in real time.

Creation of a porous electrode

The electrode array consisted of electrochemically treated platinum bulk electrodes. Each electrode was bullet shaped and created by a lathe from a bulk 0.5-mm-diameter platinum bar [14]. Electrochemical etching was done to create a porous surface that would allow for a high charge injection capacity. Electrochemical etching was done by applying a +5-volt DC to the electrode for 1 s, followed by −5-volt DC for another 1 s. The entire process was performed with the electrode immersed in phosphate-buffered saline (PBS) [14]. This voltage cycle was repeated for 15.5 h at room temperature. Each electrode was 0.5 mm in diameter and 0.3 mm in height (Fig. 1a, b).

Before stimulating the retina with the porous electrode, the effects of the porous surface treatment were evaluated by measuring the impedance and performing a spectroscopic analysis of porous and nonporous electrodes. These measurements were performed with the electrodes immersed in PBS at room temperature. The surface geometry of the electrodes was examined with a scanning electron microscope (SEM). We measured electrode charge injection capacity, which is defined as the maximum charge density capacity without deviation of the platinum water window [−0.6 to +0.8 V vs. silver/silver chloride (Ag/AgCl)] during the charge injection. Current pulses consisted of 500-µs duration and cathodic-first pulses at 30 Hz for measurements. We created an electrode array to deliver electrical stimulation to the retina. Each array comprised two porous electrodes with a center-to-center distance of 1.5 mm (Fig. 1c). The basal plate of the electrode array was made of paryline.

Electrical stimulation of the retina

To implant the electrode array, a horizontal skin incision was made about 20 mm from the lateral canthus. The temporal orbital bone was removed to expose the sclera, and the lateral rectus muscle and retractor oculi muscle were cut. A scleral pocket incision of approximately 5 × 5 mm was made with a crescent knife in the superotemporal area 15 mm from the corneal limbus and just above the long posterior ciliary artery. The electrode array was inserted into the scleral pocket. The lead wire was sutured to the scleral surface. A silver plate (5 × 10 mm) was placed under the scalp as the return electrode. After electrode array implantation, optical coherence tomography (OCT) images of the posterior pole of the eye in the implantation area were obtained with iVue (Optovue, Fremont, CA, USA). This OCT device captures cross-sectional images of the retina and choroid. We evaluated the height of the lump created by the electrode (Fig. 7c). OCT examinations were performed on cat nos. 3, 4, 5, 6, and 7. Impedance between the stimulating and return electrode was measured at 1 kHz using an LCR meter (chemical impedance meter 3532-80; HIOKI, Ueda Japan) on all cats. Impedances were measured just before and 1, 4, and 17 h after onset of the stimulation trial. For each trial, 4-s pulse trains were delivered to the retina. The pulse trains consisted of cathodic-first biphasic pulses with a frequency of 20 Hz, and pulse duration/phase was 0.5 ms. Cathodic-first biphasic pulses were used in part because their charge injection capacity is higher than that of anodic-first biphasic pulses [13]. To determine the correlation between the stimulus current and the area of reflectance changes, the electrical current was systematically increased from 0.03 to 2.0 mA. All stimulating pulses were generated using an STG4008 stimulator (Multi Channel Systems MCS, Reutlingen, Germany). The mass-evoked potential at the optic chiasm stimulated by STS was monitored on an oscilloscope to confirm the effectiveness of the electrical stimulation.

Histologic analyses

Histologic studies were performed on cat nos. 4, 5, 6, and 7 to evaluate scleral thickness where the electrode array was inserted. After the experiments, the electrode array was removed from the eye, and the cat was deeply anesthetized with pentobarbital sodium (somnopentyl; Kyoritsu Seiyaku, Tokyo, Japan). The eye was enucleated and fixed in 2 % paraformaldehyde and 1.25 % glutaraldehyde in PBS. The eye was embedded in paraffin and cut into 7-μm-thick sections, which were then stained with hematoxylin and eosin (H&S) and examined by light microscopy. Scleral thickness was measured in sections passing through the area of electrode-array implantation.

Data analyses

As mentioned previously, a 2D map of reflectance changes was obtained by subtracting raw fundus images taken before from those taken after stimulation. To minimize the effect of blood vessel responses, we analyzed an area of 100 × 100 pixels around the position of the stimulating electrode (Fig. 2a). Positions were identified using raw fundus images. We superimposed the fundus image onto the 2D map of reflectance change and plotted electrode positions on the map.

To evaluate the change in area of reflectance, a GSV of 20 was set as the cutoff to reduce the effect of baseline fluctuations in the 2D map. This value was approximately 4 standard deviations (SD) of the GSV without stimulation. To study the relationship between reflectance change and current amplitude, we summed the GSVs of all pixels in the selected area. This value was named the integrated GSV and used as an indicator of the amplitude of reflectance change. These analyses were performed with Matlab (The MathWorks, Natick, MA, USA) and OriginPro (version 8.5; OriginLab, Northampton, MA, USA). To determine the centroid of reflectance changes, a 2D map of the reflectance changes was converted to intensity images, the GSV of which represented the absolute value of the reflectance change (Fig. 2b). Intensity images were then converted to binary images (Fig. 2c). The threshold level for binarization was adjusted to 30 % of maximum GSV. Using the binary image, the centroid of the white-pixels region was calculated using the Image Processing Toolbox for Matlab. Next, we calculated the ellipse that had the same normalized second central moments as the white-pixels region of the binary images. Cross sections of intensity images were computed along the major and minor axes of the ellipse on intensity images (Fig. 2d). To evaluate the spatial extent of reflectance changes, cross sections were fitted to a Gaussian peak function (Fig. 2e, f), and the full width at half maximum (FWHM) was computed using OriginPro. In some cases, the signal of reflectance change was low, and Gaussian fitting was not possible. In such cases, evaluation of major and minor axes of the ellipse was not done. The Pearson product moment correlation was used to examine the correlation between threshold and other factors. A probability value of <0.05 was considered significant. All statistical analyses were performed using JMP version 9.0 software (SAS Institute, Cary, NC, USA).

Results

Evaluation of porous surface treatment

Scanning electron microscopy confirmed that our surface treatment resulted in a highly pitted surface (Fig. 1a).

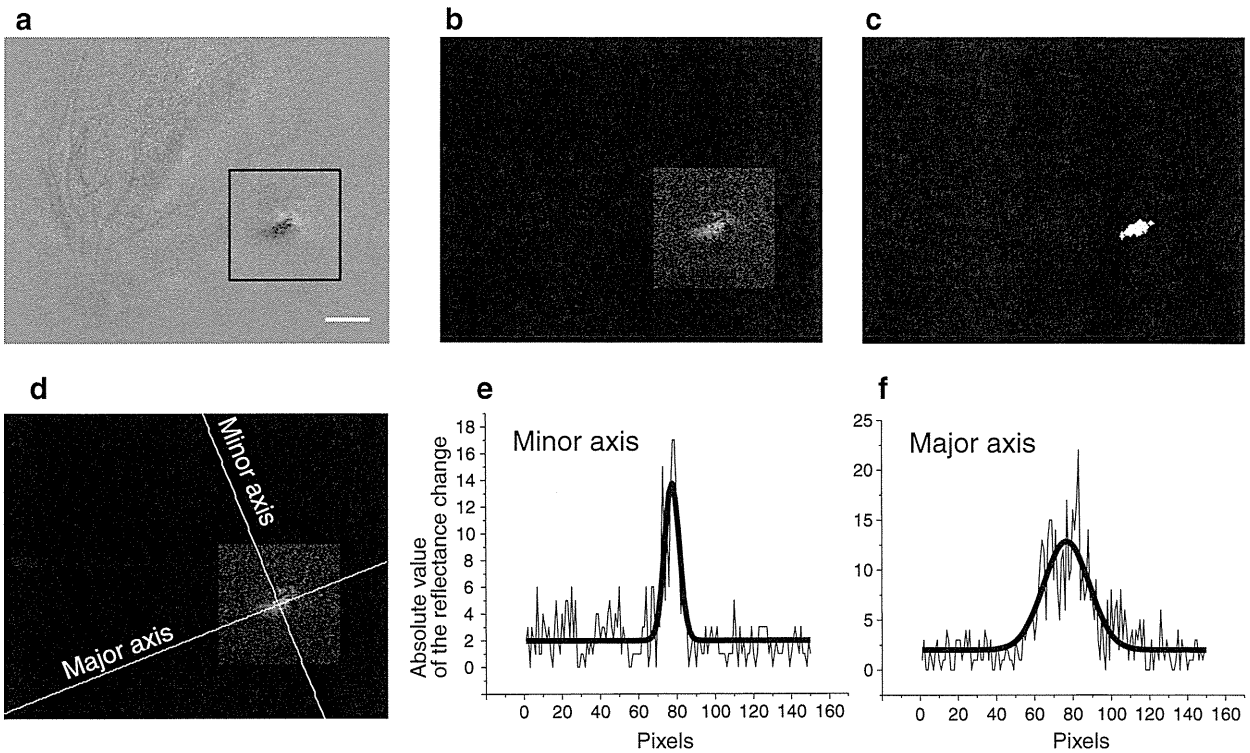

Fig. 2 Calculation of amplitude and spatial extent of reflectance change. **a** Two-dimensional map of reflectance changes 2.0 s after onset of electrical stimulation. To minimize the effect of blood vessel responses, we analyzed areas of 100 × 100 pixels around the electrode array position (*bold line*). *Scale bar* 1 mm. **b** Changes in reflectance in which the absolute value of reflectance change beyond the cutoff value is shown. This image was calculated from (**a**). **c** Intensity image was converted to a binary image. **d** Major and minor axes of the ellipse calculated from (**c**). **e**, **f** Cross sections of grayscale values on the map of absolute value of reflectance changes (**e**, cross section on the major axis; **f**, cross section on the minor axis). The *bold lines* are approximate curves fitted to a Gaussian peak function

Images showed that the pits (size range 1–10 μm) were uniformly distributed along the surface of the platinum bar. In an in vitro impedance test, we observed a three- to tenfold decrease in electrode impedance after the etching process (Fig. 1d). Charge injection capacity of the porous electrode was 1.12 μC/phase in PBS, which was eight times larger than that of the nonporous electrode. These observations demonstrated that the pitted surface increased the electrode surface area.

Time course of reflectance changes in response to electrical stimulation

Examination of the 2D map of reflectance changes after electrical stimulation showed changes in the retinal area where the tip of the electrode adhered to the choroid (Fig. 3a). In a representative case, reflectance change peaked at 2.0–2.5 s after stimulus onset, was sustained for 3.0 s, and then decreased (Fig. 3b). Reflectance changes were observed around blood vessels at about 5.0 s after stimulation onset and about 3.0 s after general reflectance change onset (Fig. 3a).

Electrophysiologic recordings from the optic chiasm following electrical stimulation

The amplitude of electrically evoked potentials recorded in the optic chiasm increased with an increase in stimulus current (Fig. 4a, b). The amplitude of the electrically evoked potential was determined by the first negative peak (latency approximately 3 ms) and the second positive peak (latency approximately 4 ms) (Fig. 4a). The relationship between the amplitude of the electrically evoked potential and the integrated GSV of reflectance changes was assessed in cat no. 5 (electrode Ch 2). Linear regression analysis showed a value of $R^2 = 0.99$, suggesting that reflectance changed linearly with the amplitude of the electrically evoked potential at the optic chiasm (Fig. 4c).

Relationship between reflectance changes and current intensities

The area of reflectance changes increased with currents exceeding the threshold value (Fig. 5a; cat no. 5, electrode Ch1). The integrated GSV of reflectance changes increased

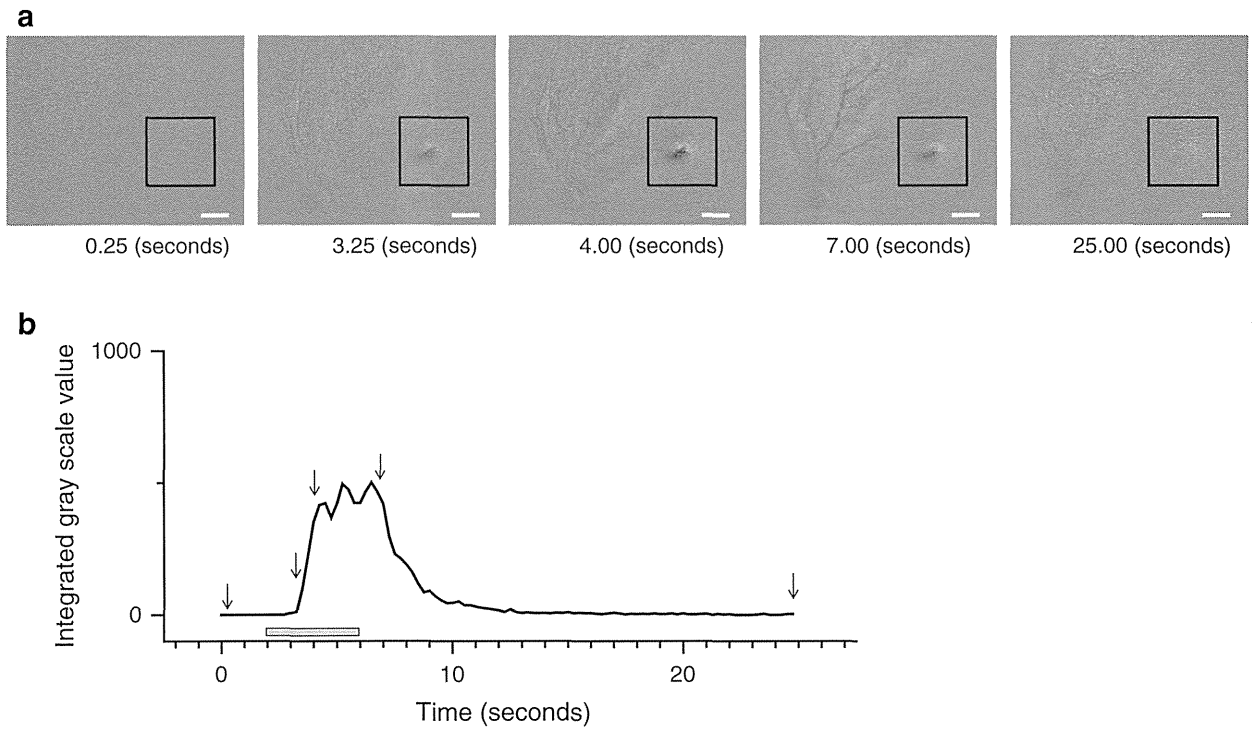

Fig. 3 Time course of reflectance changes after electrical stimulation of the retina. **a** Two-dimensional map of reflectance change at 0.25, 3.25, 4.00, 7.00, and 25.00 s into the trial. Electrical stimulation was applied from between 2.00 and 6.00 s into the trial. Data obtained from cat no. 1, tested with a current of 0.7 mA. The *black square* indicates the area of analysis. *Scale bar* 1 mm. **b** Time course of intensity of integrated gray-scale values of reflectance changes. The *arrows* indicate times when data shown in **a** were obtained. The *gray bar* indicates stimulation period

with an increase in stimulating current (Fig. 5b, c). The threshold current varied among electrodes (410 ± 440 μA; mean ± SD; Fig. 5c) and were defined as the minimum current that evoked a reflectance change of at least 200 integrated GSV.

Area of reflectance changes after electrical stimulation

The average area of reflectance change after a stimulating current of a 1.5 × threshold was 0.42 ± 0.23 mm along the minor axis and 1.46 ± 0.86 mm along the major axis (Table 1). When two different retinal loci were stimulated by passing currents through two different electrodes of the array, distribution of localized signals changed (Fig. 6a–c; cat no. 1). The average distance between the two geometrical centers of retinal reflectance changes was 1.69 ± 0.38 mm when the distance between the two electrodes was 1.5 mm (Table 2).

Relationship between scleral thickness and threshold

The thickness of the sclera on the choroidal side was measured in histologic sections taken through the scleral pocket (Fig. 7a). The threshold current increased with an increase in scleral thickness ($P = 0.0002$; $R^2 = 0.9215$; Fig. 7b).

Relationship between lump height created by the electrode and threshold current

The height of the lump created by the electrode was measured in OCT images (Fig. 7c). Our analysis showed that the threshold current decreased with an increase in lump height created by the electrode array ($P = 0.0111$; $R^2 = 0.6259$; Fig. 7d).

Relationship between impedance and threshold current

The time course of the impedance between the stimulating electrode and the return electrode in vivo showed that the impedance was stable throughout the stimulating trials for up to 17 h. To evaluate the relationship between impedance and threshold current, impedances were measured 15–17 h after onset of the stimulating trial; threshold current decreased with an increase in impedance ($P = 0.0147$; $R^2 = 0.2554$; Fig. 8).

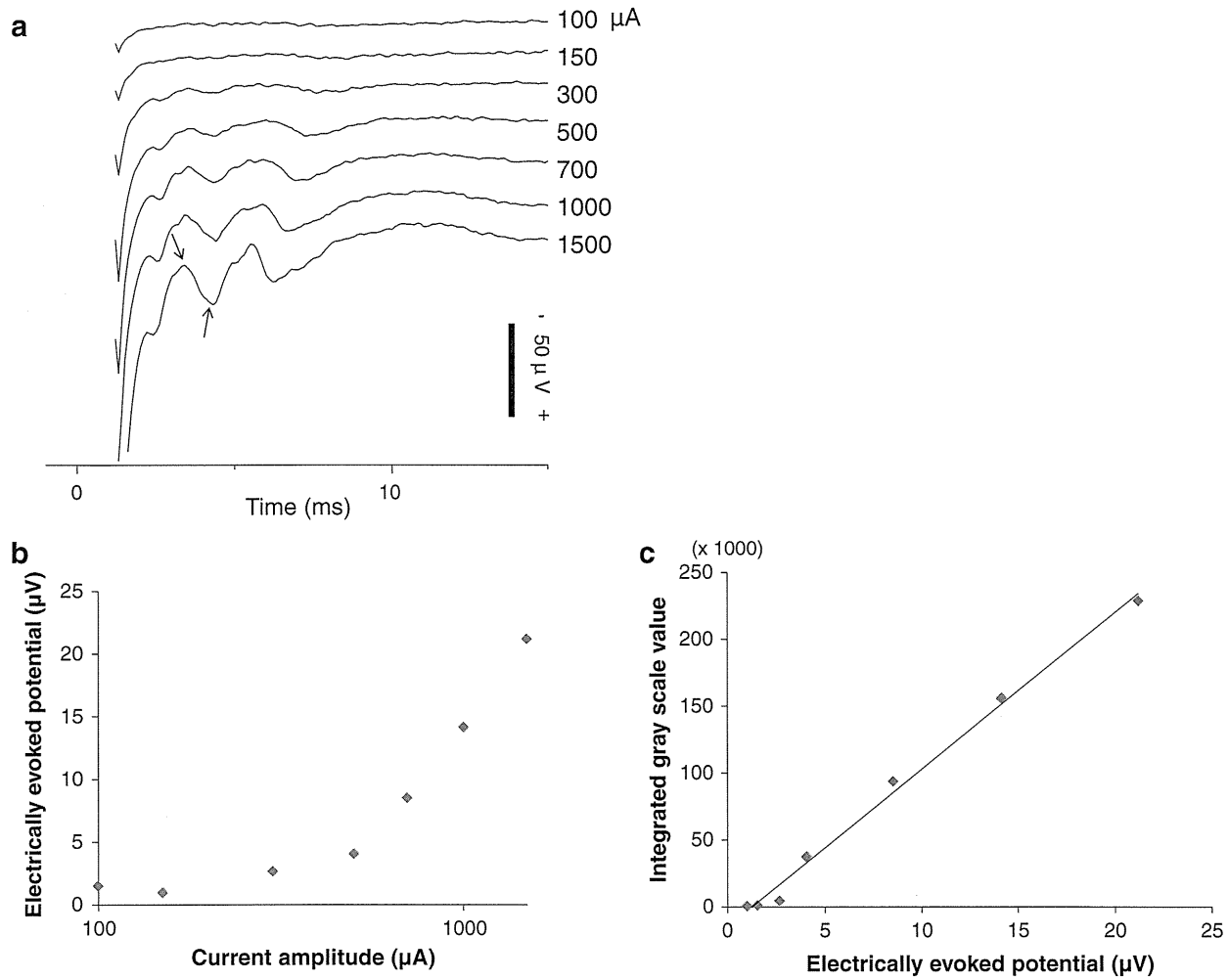

Fig. 4 Potentials evoked by electrical stimulation with the etched electrode in the suprachoroidal–transretinal stimulation (STS) array and recorded at the optic chiasm. **a** Typical electrically evoked potentials recorded at the optic chiasm in response to retinal stimulation. The *left arrow* indicates the first negative peak and the *right arrow* the second positive peak. Data were obtained from cat no. 5 and with electrode Ch2 stimulation. **b** Relationship between the amplitude of electrically evoked potentials and current amplitude. **c** Relationship between integrated gray-scale values of reflectance changes and electrically evoked potentials. The equation for the regression line on the graph is $y = 11{,}728 \text{ x } -14{,}411$ ($R^2 = 0.99$)

Discussion

Previously, we examined the effect of electrical stimulation by a single platinum electrode on the retina using the retinal intrinsic signal in cats and found that electrical currents effectively stimulated local areas of the retina [18]. In the study reported here, we examined the effect of an array of electrochemically treated bulk electrodes (Fig. 1) on eliciting the retinal intrinsic signal. The electrode array was implanted in a scleral pocket, and the procedures were similar to those used in clinical trials [6, 11]. The time course of reflectance changes was relatively slow and similar to that reported previously [18, 19], indicating that reflectance changes do not directly reflect retinal neuronal activity but may be related to vasodynamic processes secondary to excitation of retinal neurons [19] (Fig. 3). The amplitude of the electrically evoked potential at the optic chiasm was significantly correlated with the integrated GSV of reflectance changes, suggesting that the integrated GSV reflected retinal neuronal activity (Fig. 4). The threshold current for reflectance changes varied among eyes, indicating that differences in electrode placement, e.g., distance from the retina and degree of electrical contact to the sclera, might affect the strength of the electrical current that passes to the retina (Fig. 5).

We also stimulated two retinal sites 1.5-mm apart, which resulted in two different retinal areas that responded to stimuli. The distance between centroids of reflectance

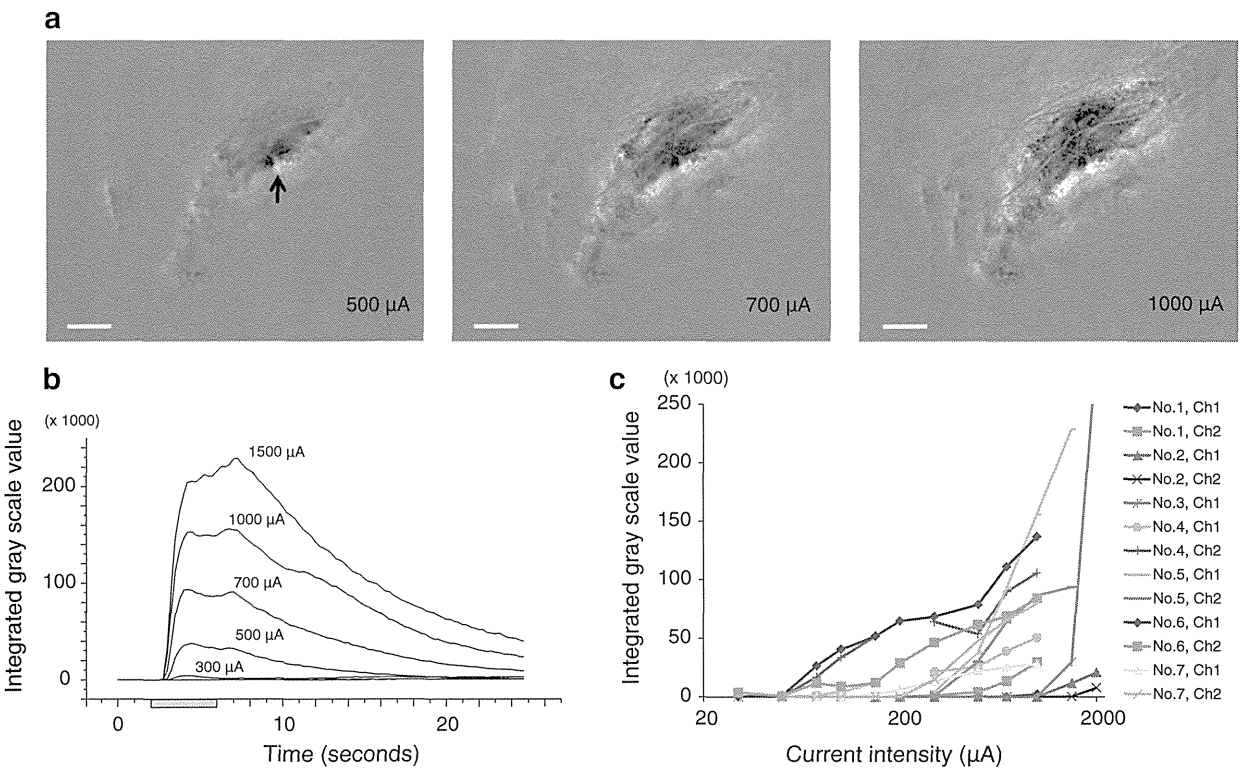

Fig. 5 Relationship between reflectance changes and stimulus currents. **a** Two-dimensional map of reflectance changes 2.00 s after the onset of electrical stimulation with current intensities of 500, 700, and 1,000 μA. The *black arrow* indicates the position of the stimulating electrode. *Scale bar* 1 mm. **b** Intensity time course of integrated gray-scale values (GSV) of reflectance changes. **c** Relationship between integrated GSV of reflectance changes and stimulus current intensities

Table 1 Spatial distributions of reflectance changes

Cat number	Electrode number	Current (μA)[a]	FWHM (mm)	
			Short axis	Long axis
1	Ch1	700	0.29	0.93
1	Ch2	300	0.47	1.20
2	Ch1	1500	0.37	1.51
3	Ch1	1500	0.45	1.61
4	Ch1	100	0.60	3.45
4	Ch2	75	0.16	0.89
5	Ch1	500	0.93	1.34
5	Ch2	500	0.14	0.53
6	Ch1	75	0.31	2.29
7	Ch1	150	0.44	0.80

FWHM full width at half maximum

[a] This current represents a stimulating current of 1.5 × threshold

Table 2 Two-point discrimination

Cat number	Distance between centroids (mm)
1	2.09
4	1.34
5	1.64

changes elicited by the two stimulating electrodes averaged 1.69 mm and was comparable with the distance between the two electrodes. This indicated that two different stimulating sites with a distance of at least 1.5 mm can evoke discriminated responses in the retina using the porous electrode. According to the Gullstrand theoretical exact eye, the length from the nodal point to the retina is approximately 17 mm. Therefore, the distance of 1.5 mm in the human retina corresponds to visual angles of approximately 5.0°, which is equivalent to a visual acuity of 2.5 logMAR units.

In the best result of this study, the FWHM was 0.14 mm along the minor axis and 0.53 mm along the major axis, which correspond to visual angles of approximately 0.5° and 1.8°, respectively. This was comparable with the diameter of the stimulating electrode (0.5 mm). Downsizing the electrode diameter may improve the spatial resolution under optimal conditions.

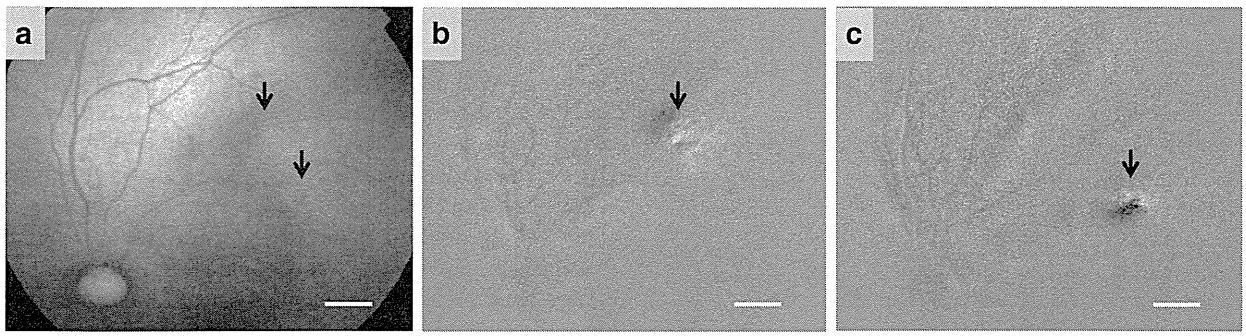

Fig. 6 Reflectance changes in response to electrical stimulation at different retinal loci. **a** Fundus photograph of cat retina. The *left arrow* indicates the position of electrode Ch1 electrode and the *right arrow* the position of the Ch2 electrode. *Scale bar* 1 mm. **b**, **c** Two-dimensional map of reflectance changes 2.0 s after the onset of electrical stimulation (**b** Ch2, 300 μA; **c** Ch1, 700 μA)

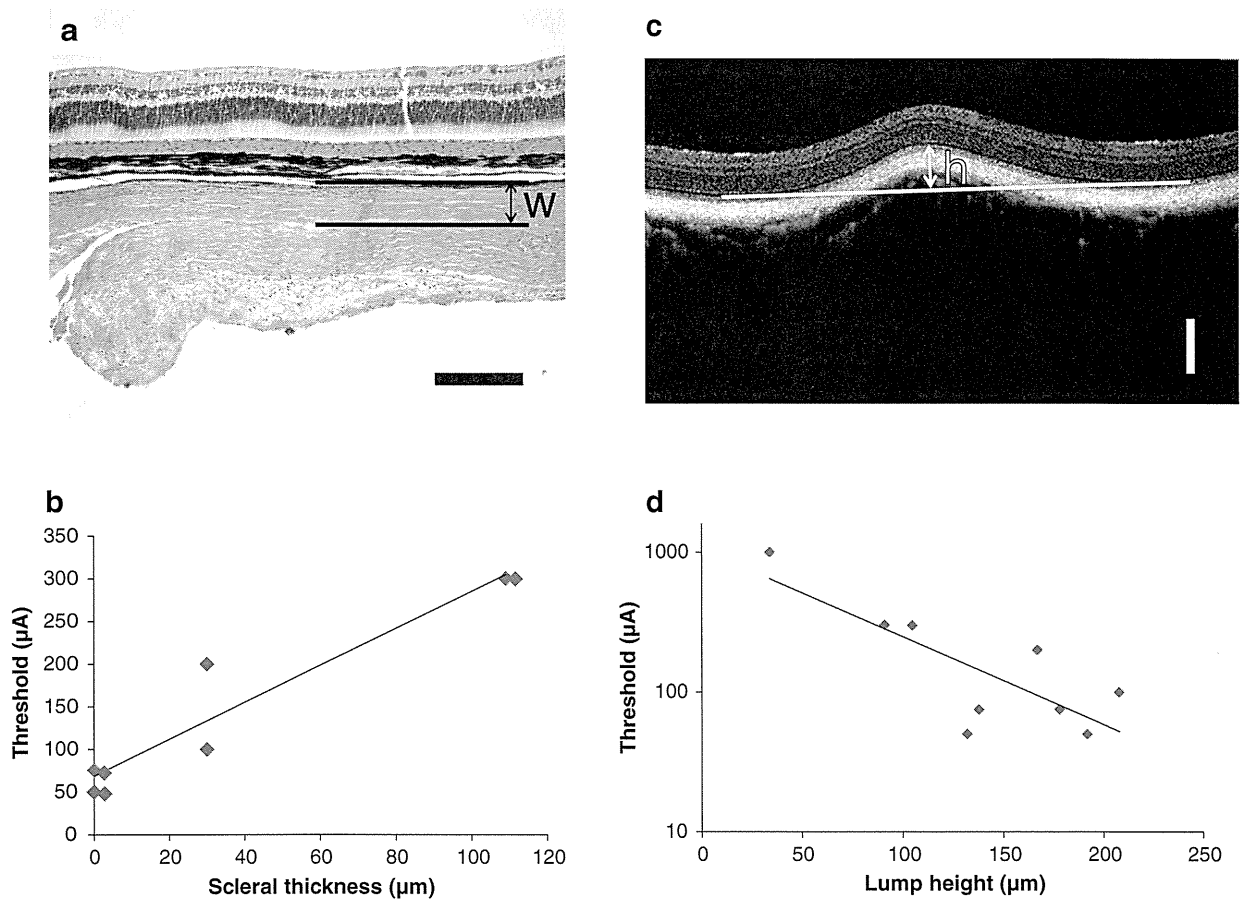

Fig. 7 **a**, **b** Relationship between threshold current and scleral thickness on histology or **c**, **d** lump height on optical coherence tomography (OCT). **a** Histology of retina and sclera where the electrode array was implanted: *w* scleral thickness between scleral pocket and choroid. **b** Relationship between scleral thickness and threshold current. The equation for the regression line is $y = 2.1657x + 68.493$ ($R^2 = 0.92$). **c** OCT image of the retina at electrode position. The height of the lump (*h*), created by the implanted electrode, was obtained from the inner- and outer-segment (IS/OS) line and defined as peak height from baseline. The baseline was a horizontal line (*white line* in **c**), obtained from the tangent of the IS/OS line. *Scale bar* 200 μm. **d** Relationship between lump height and threshold current. The equation for the regression line is $y = 1059.6e^{-0.014x}$ ($R^2 = 0.6259$)

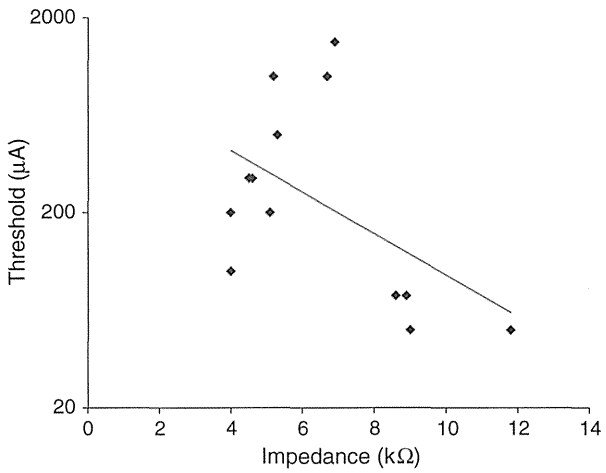

Fig. 8 Relationship between electrode impedance and threshold current. Impedance data were obtained from all cats. The equation for the regression line is $y = 1110.8e^{-0.245x}$ ($R^2 = 0.2554$)

Retinal Implant has created a subretinal prosthesis, which is being tested in clinical trials. Zrenner et al. [2] reported a visual acuity as high as 1.43 logMAR units with this prosthesis. The Argus II retinal prosthesis, from Second Sight Medical Products, is an epiretinal prosthesis and is also being evaluated in a clinical trial. Humayun et al. [5] reported that the best recorded visual acuity with this prosthesis was 1.8 logMAR units. Although it is difficult to compare findings among different clinical trials and in vivo studies, our results suggest that under optimal conditions, e.g., sufficient scleral thickness, STS would allow patients to achieve levels of resolution comparable with those obtained using epiretinal or subretinal prostheses. Furthermore, the electrodes were used to inject 1.12-μC/phase current pulses without exceeding the water window in PBS. This corresponds to 2.2 mA over a 0.5-ms pulse duration. The threshold for retinal response to the STS with the porous electrode was lower than the injection limit. Therefore, the porous electrode can be used effectively to stimulate an STS retinal prosthesis. The threshold current was lower when the thickness of the scleral tissue between the electrode and retina was thinner, indicating that the retina is more effectively stimulated when electrodes are situated closer to the retina (Fig. 7). However, it should be noted that mechanical damage to the retina could be observed when scleral thickness was <80 μm in rabbit experiments (data not shown). Therefore, a balance between scleral tunnel depth and current safety should be obtained. The scleral pocket was surgically created with a crescent knife. However, it is difficult to create a constant scleral pocket depth in every surgical operation. Therefore, residual scleral thicknesses on the electrode surface varied from 0 to 0.1 mm.

Electrode pressure against the choroid and retina was not the same for all experiments. Pressure was affected by scleral pocket depth, width and scleral thickness. For example, pressure was weak when the scleral pocket was wide. Threshold current was lower when the lump created by the underlying electrode was high or electrode impedance was high, which would indicate that a better contact between electrode and sclera may increase electrode impedance. The observation that better contact between electrode and sclera might increase impedance is consistent with reported data [20, 21]. These findings should be useful in creating the optimal scleral pocket.

An advantage of the porous electrode is its high durability. The charge injection capacity of a porous electrode was reportedly kept stable for 1 month of chronic implantation in rabbits [22]. In the study reported here, impedance was also stable throughout the stimulation trials for up to 17 h. These results suggest that porous electrodes have adequate durability for long-term implantation. To demonstrate the superiority of porous electrodes, it may be advisable to compare the difference in results between nonporous and porous electrodes in an in vivo experiment. However, the threshold or localization of response to STS using these electrodes varied with scleral pocket thickness and contact conditions. Therefore, we evaluated the spatial distribution and threshold of neural responses evoked by porous electrodes only. For further comparison of porous and nonporous electrodes, we intend to fabricate a special electrode array.

In conclusion, electrochemically treated porous platinum electrodes are effective in stimulating localized areas of the retina when implanted in a scleral pocket. The threshold current to stimulate the retina was influenced by the thickness of the residual sclera and the firmness of the contact between electrodes and adjacent sclera.

Acknowledgments This study was supported by the Strategic Research Program for Brain Sciences and by a Grant-in-Aid for Scientific Research (A22249058) from the Japanese Ministry of Education, Culture, Sports, Science and Technology, and by a Health Sciences Research Grant (H24-Medical Device004) from the Japanese Ministry of Health, Labor and Welfare.

Conflicts of interest H. Kanda, Grant (NIDEK); T. Mihashi, None; T. Miyoshi, None; Y. Hirohara, Employee (Topcon); T. Morimoto, None; Y. Terasawa, Employee (NIDEK); T. Fujikado, Grant (NIDEK).

References

1. Zrenner E, Bartz-Schmidt KU, Benav H, Besch D, Bruckmann A, Gabel VP, et al. Subretinal electronic chips allow blind patients to read letters and combine them to words. Proc Biol Sci. 2011;278:1489–97.
2. Stingl K, Bartz-Schmidt KU, Besch D, Braun A, Bruckmann A, Gekeler F, et al. Artificial vision with wirelessly powered

subretinal electronic implant alpha-IMS. Proc Biol Sci. 2013;280:20130077.
3. Zrenner E. Will retinal implants restore vision? Science. 2002;295:1022–5.
4. Humayun MS, Weiland JD, Fujii GY, Greenberg R, Williamson R, Little J, et al. Visual perception in a blind subject with a chronic microelectronic retinal prosthesis. Vision Res. 2003;43:2573–81.
5. Humayun MS, Dorn JD, da Cruz L, Dagnelie G, Sahel JA, Stanga PE, et al. Interim results from the international trial of second sight's visual prosthesis. Ophthalmology. 2012;119:779–88.
6. Fujikado T, Morimoto T, Kanda H, Kusaka S, Nakauchi K, Ozawa M, et al. Evaluation of phosphenes elicited by extraocular stimulation in normals and by suprachoroidal-transretinal stimulation in patients with retinitis pigmentosa. Graefes Arch Clin Exp Ophthalmol. 2007;245:1411–9.
7. Kanda H, Morimoto T, Fujikado T, Tano Y, Fukuda Y, Sawai H. Electrophysiological studies of the feasibility of suprachoroidal-transretinal stimulation for artificial vision in normal and RCS rats. Invest Ophthalmol Vis Sci. 2004;45:560–6.
8. Nakauchi K, Fujikado T, Kanda H, Morimoto T, Choi JS, Ikuno Y, et al. Transretinal electrical stimulation by an intrascleral multichannel electrode array in rabbit eyes. Graefes Arch Clin Exp Ophthalmol. 2005;243:169–74.
9. Sakaguchi H, Fujikado T, Fang XY, Kanda H, Osanai M, Nakauchi K, et al. Transretinal electrical stimulation with a suprachoroidal multichannel electrode in rabbit eyes. Jpn J Ophthalmol. 2004;48:256–61.
10. Nakauchi K, Fujikado T, Kanda H, Kusaka S, Ozawa M, Sakaguchi H, et al. Threshold suprachoroidal-transretinal stimulation current resulting in retinal damage in rabbits. J Neural Eng. 2007;4:S50–7.
11. Fujikado T, Kamei M, Sakaguchi H, Kanda H, Morimoto T, Ikuno Y, et al. Testing of semi-chronically implanted retinal prosthesis by suprachoroidal-transretinal stimulation in patients with retinitis pigmentosa. Invest Ophthalmol Vis Sci. 2011;52:4726–33.
12. Cogan SF. Neural stimulation and recording electrodes. Annu Rev Biomed Eng. 2008;10:275–309.
13. Terasawa Y, Osawa K, Ozawa M, Tokuda T, Ohta J, Tano Y. Large-surface-area electrodes based on bulk micromachining. Invest Ophthalmol Vis Sci. 2008;49:3020.
14. Terasawa Y, Tashiro H, Osawa K, Yabusaki A, Ozawa M, Noda T, et al. Characterization of electrochemically-treated platinum bulk electrodes. Invest Ophthalmol Vis Sci. 2010;51:3033.
15. Stett A, Barth W, Weiss S, Haemmerle H, Zrenner E. Electrical multisite stimulation of the isolated chicken retina. Vision Res. 2000;40:1785–95.
16. Cicione R, Shivdasani MN, Fallon JB, Luu CD, Allen PJ, Rathbone GD, et al. Visual cortex responses to suprachoroidal electrical stimulation of the retina: effects of electrode return configuration. J Neural Eng. 2012;9:036009.
17. Eckhorn R, Wilms M, Schanze T, Eger M, Hesse L, Eysel UT, et al. Visual resolution with retinal implants estimated from recordings in cat visual cortex. Vision Res. 2006;46:2675–90.
18. Okawa Y, Fujikado T, Miyoshi T, Sawai H, Kusaka S, Mihashi T, et al. Optical imaging to evaluate retinal activation by electrical currents using suprachoroidal-transretinal stimulation. Invest Ophthalmol Vis Sci. 2007;48:4777–84.
19. Mihashi T, Okawa Y, Miyoshi T, Kitaguchi Y, Hirohara Y, Fujikado T. Comparing retinal reflectance changes elicited by transcorneal electrical retinal stimulation with those of optic chiasma stimulation in cats. Jpn J Ophthalmol. 2011;55:49–56.
20. Ray A, Chan LLH, Gonzalez A, Humayun MS, Weiland JD. Impedance as a method to sense proximity at the electrode-retina interface. IEEE Trans Neural Syst Rehabil Eng. 2011;19:696–9.
21. de Balthasar C, Patel S, Roy A, Freda R, Greenwald S, Horsager A, et al. Factors affecting perceptual thresholds in epiretinal prostheses. Invest Ophthalmol Vis Sci. 2008;49:2303–14.
22. Terasawa Y, Tashiro H, Nakano Y, Osawa K, Ozawa M. Safety assessment of semichronic suprachoroidal electrical stimulation to rabbit retina. Conf Proc IEEE Eng Med Biol Soc. 2013;2013:3567–70.

SCLERAL IMBRICATION COMBINED WITH VITRECTOMY AND GAS TAMPONADE FOR REFRACTORY MACULAR HOLE RETINAL DETACHMENT ASSOCIATED WITH HIGH MYOPIA

MASATO FUJIKAWA, MD, HAJIME KAWAMURA, MD, MASASHI KAKINOKI, MD, OSAMU SAWADA, MD, TOMOKO SAWADA, MD, YOSHITSUGU SAISHIN, MD, MASAHITO OHJI, MD

Purpose: To evaluate scleral imbrication with vitrectomy and gas tamponade for refractory macular hole retinal detachment associated with high myopia.

Methods: We retrospectively reviewed the medical records of eight eyes with macular hole retinal detachment and high myopia treated with temporal scleral imbrication, pars plana vitrectomy, and gas tamponade for refractory macular hole retinal detachment with history of pars plana vitrectomy. Retinal reattachment and macular hole closure were assessed. Postoperative changes in axial length and surgically induced astigmatism were evaluated.

Results: The retinas were reattached in all eyes and the macular holes closed in 6 (75%) eyes. The mean baseline logarithm of the minimum angle of resolution best-corrected visual acuity of 1.43 ± 0.48 significantly ($P < 0.01$) improved to 0.87 ± 0.34 at the final visit (889 ± 173 postoperative days). The mean baseline axial length of 29.5 ± 1.3 mm decreased significantly ($P < 0.01$) to 27.1 ± 1.9 mm 1 month after scleral imbrication and 28.1 ± 1.7 mm at the final visit ($P < 0.05$ vs. baseline, $P = 0.13$ vs. 1 month). The mean 1-month surgically induced astigmatism of 3.6 ± 1.4 diopters (D) after scleral imbrication significantly ($P < 0.05$) decreased to 2.4 ± 1.5 D at the final visit.

Conclusion: Scleral imbrication with vitrectomy and gas tamponade resulted in high reattachment and macular hole closure rates for treating refractory macular hole retinal detachment.

RETINA 34:2451–2457, 2014

Macular holes (MHs) are common in highly myopic eyes and are often associated with retinal detachments. Various surgical techniques have been studied to treat macular hole retinal detachment (MHRD) in highly myopic eyes. Since Gonvers and Machemer reported using pars plana vitrectomy (PPV) and gas tamponade in 1982, many surgical treatments including intravitreal injection of gas, scleral resection or imbrication, pneumatic retinopexy, PPV with silicone oil tamponade, and episcleral macular buckling have been proposed to treat MHRD.[1–7]

The most common procedure used currently is PPV with gas tamponade with the removal of epiretinal membrane and/or internal limiting membrane (ILM) in the posterior pole. Recent case series indicate that PPV and ILM peeling achieve a retinal reattachment rate ranging between 69% and 95.9% and a macular closure rate ranging between 44% and 90.7%.[8,9]

It has been suggested that a sclera that is long compared with the retina as a result of deepening of the posterior staphyloma causes failure of MH closure or retinal redetachment after treatment of MHRD in highly myopic eyes. Based on this theory, several studies have reported the efficacy of scleral resection

From the Department of Ophthalmology, Shiga University of Medical Science, Otsu, Japan.

Supported in part by a grant from the Ministry of Education, Culture, Sports, Science and Technology of Japan (#24592668) and a grant from the Ministry of Health, Labor, and Welfare.

None of the authors have any conflicting interests to disclose.

Reprint requests: Masato Fujikawa, MD, Department of Ophthalmology, Shiga University of Medical Science, Seta Tsukinowacho, Otsu 520-2192, Japan; e-mail: fujikawa@belle.shiga-med.ac.jp

combined with PPV and gas tamponade for complete retinal reattachment.[10–12] Matsuo et al[13] then simplified this technique by scleral imbrication technique together with PPV and gas tamponade. Since then, no studies have used this technique to treat MHRD in highly myopic eyes.

In this study, we performed PPV and gas tamponade with the scleral imbrication technique, especially for refractory MHRD associated with high myopia, and assessed the anatomical and functional results over the long term.

Patients and Methods

The medical records of 46 patients with MHRD associated with high myopia treated from April 2005 to March 2011 in Shiga University of Medical Science Hospital were reviewed retrospectively. Eyes with history of ocular trauma, proliferative vitreoretinopathy, and sustained silicone oil tamponade were excluded. The inclusion criterion was a record of scleral imbrication combined with PPV and gas tamponade for MHRD followed more than 6 months.

The surgery included a standard 3-port PPV with 20- or 23-gauge system under topical anesthesia. The cataract extraction and ILM peeling had been performed at the initial surgery. The remnant of ILM in the macular area was assessed using 0.25% indocyanine green (Ophthagreen; Santen Pharmaceutical Co, Ltd, Osaka, Japan) and was peeled by the vitreous forceps if detected at reoperation. Scleral imbrication was performed by placing 8.0-mm wide bites of 5-0 polyester mattress sutures (Dacron; Alcon, Fort Worth, TX); 3 mattress sutures were placed in each of the superotemporal and inferotemporal quadrants, for a total of 6 mattress sutures in an eye, followed by fluid–gas exchange using 20% sulfur hexafluoride gas (ISPAN SF_6 Intraocular Gas; Alcon, Fort Worth, TX) with aspiration of the subretinal fluid through the MH.

Retinal reattachment and MH closure were assessed using optical coherence tomography (OCT) (Cirrus OCT; Carl Zeiss Meditec, Jena, Germany). Patients were instructed to keep face-down posture after vitrectomy until the intraocular gas decreased to <50% to detect retinal reattachment by OCT. It was around 10 days. The best-corrected visual acuity (BCVA) values measured with the Landolt C chart were converted to the logarithm of the minimum angle of resolution (logMAR) for statistical analysis. A BCVA of counting fingers was defined as logMAR 2.00 according to a previous report.[14] The axial length was measured by optical coherence biometry (IOL Master; Carl Zeiss Meditec); we calculated the difference in the axial lengths between 1 month and the final visit after scleral imbrication and considered that value as the amount of rebound. Keratometric astigmatism was measured using an automated keratometer (RKT-7700 or ARK-530A; Nidek, Gamagori, Japan), and surgically induced astigmatism (SIA) was calculated by vector analysis.

Statistical analyses were performed using GraphPad Prism 6 software (GraphPad Software Inc, La Jolla, CA). The data are expressed as the mean ± SD. $P < 0.05$ was considered significant.

Results

Of the 46 eyes with MHRD, there were 7 eyes excluded based on the current criteria as follows: 1 eye with MHRD, initially performed pneumatic retinopexy, performed vitrectomy with scleral imbrication and her retina was attached but she did not followed-up after discharge; 3 eyes with MHRD remained silicone oil tamponade after vitrectomy; 2 eyes with proliferative vitreoretinopathy; 1 eye with history of ocular trauma. Of the remaining 39 eyes with MHRD, 27 eyes finally attached retina by vitrectomy with gas tamponade, 4 eyes by silicone oil tamponade followed by removal of it, and thus finally 8 eyes performed vitrectomy and gas tamponade together with scleral imbrication met the inclusion criterion. They underwent scleral imbrication together with PPV and gas tamponade as a second surgery, that is, 5 cases with redetachment of the MHRD after primary PPV with gas tamponade for MHRD; 1 case with redetachment of MHRD after primary PPV with gas tamponade followed by secondary PPV with silicone oil tamponade; 1 case with MHRD that developed 5 months after PPV for vitreomacular traction syndrome; and 1 case with MHRD that developed 1 month after PPV for MH in a highly myopic eye. The mean interval between the initial PPV and the PPV with scleral imbrication was 94.1 ± 109.5 days (range, 15–316 days), including 2 eyes performed initial PPV for a vitreomacular traction syndrome and a MH. The baseline demographics just before scleral imbrication are summarized in Table 1.

The mean follow-up period after scleral imbrication was 889 ± 173 days (range, 636–1,182 days). Visual improvement and retinal reattachment were achieved in all (100%) eyes, and MH closure was confirmed in 6 (75%) eyes by OCT without adverse events (Figure 1A). The mean logMAR BCVA was 1.43 ± 0.48 (range, 0.52–2.00) before scleral imbrication and it improved significantly ($P < 0.01$ by the paired t-test) to 0.87 ± 0.34 (range, 0.15–1.22) at the final visit (Figure 1B).

Table 1. Baseline Demographics Before Scleral Imbrication

No. patients	8
No. eyes	8
Final surgery	January 2006 to January 2011
Men/women (%)	1 (12.5%)/7 (87.5%)
Age (years)	68.4 ± 6.7 (range, 57–77)
Preoperative logMAR BCVA	1.43 ± 0.48 (range, 0.52–2.00*)
Axial length (mm)	29.5 ± 1.3† (range, 27.5–31.7)

*Counting fingers is defined as 2.00 logMAR.
†n = 6.

The representative color fundus photographs and OCT images were shown in Figures 2 and 3, respectively. Imbricated shape of temporal eye wall was sustained during follow-up period (Figure 2). Optical coherence tomography images were taken before and after scleral imbrication in four eyes. The convexity of posterior eye wall including posterior staphyloma was flattened after scleral imbrication, and the shape was sustained to final visit (Figure 3).

Axial length data before scleral imbrication were unavailable for two of the eight eyes. In the 6 eyes in which preoperative and postoperative axial lengths were measured, the axial lengths shortened in all eyes after scleral imbrication (Figure 4A). The mean axial length was 29.5 ± 1.3 mm (range, 27.5–31.7 mm; n = 6) just before scleral imbrication and it decreased significantly ($P < 0.01$ by the paired t-test) to 26.7 ± 1.9 mm (range, 24.9–29.2 mm; n = 6) 1 month after scleral imbrication. The mean percent decrease in axial length at 1 month after scleral imbrication was 9.6 ± 4.0% (Figure 4B). The mean axial length at the final visit was 28.1 ± 1.7 mm (range, 25.7–31.0 mm; n = 8), which was significantly ($P < 0.05$ by the paired t-test; n = 6) shorter than before; the change did not reach significance ($P = 0.13$ by the paired t-test; n = 8) compared with that 1 month after scleral imbrication (Figure 4C). The mean amount of axial length shortening was 2.8 ± 1.1 mm (range, 1.4–4.4 mm; n = 6) at 1 month, and it was 1.3 ± 1.0 mm (range, 0.2–3.1 mm; n = 6) at the final visit after scleral shortening. When we analyzed the difference in the axial lengths between 1 month and the final visit after scleral imbrication, the mean rebound of the axial length was 1.0 ± 1.6 mm (range, –2.2 to 3.3 mm; n = 8). The individual changes in the axial length are shown in Table 2. The rebound of the axial length remained relatively stable over time after it was observed several months postoperatively (Figure 4A).

Pre- and postoperative Keratometric astigmatism were measured in all 8 eyes. All eyes had regular astigmatism and six of eight eyes had against-the-rule astigmatism at final visit. The mean amount of SIA was 3.6 ± 1.4 diopters (D) (range, 1.3–6.0 D) at 1 month after scleral imbrication. This decreased significantly ($P < 0.05$ by Wilcoxon matched-pairs signed-rank test) to 2.4 ± 1.5 D (range, 0.8–5.6 D) at the final visit after scleral imbrication (Figure 5). There was no correlation between the amount of rebound of the axial length and the SIA from 1 month to the final visit after scleral imbrication (Pearson's r = –0.46, $P = 0.25$).

Discussion

Before the development of the transvitreal approach, scleral imbrication made by sutures on the temporal side combined with macular diathermy was described as an effective method for treating MHRD.[15–17] Thereafter, Matsumura and Ogino[10] proposed an effective method for complete retinal reattachment, that is, scleral resection combined with vitrectomy in 1996. In 2001, Matsuo et al[13] performed a simpler method with scleral imbrication in combination with PPV and gas tamponade as a second surgery for 5 eyes with an MHRD in a pilot study and achieved retinal reattachment and MH closure in all cases. Since these pilot studies, no report using this

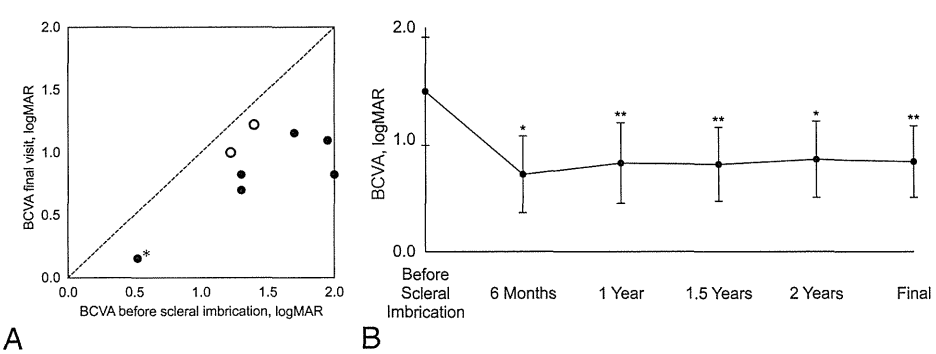

Fig. 1. A. The BCVA improved after scleral imbrication. The open and closed circles indicate open and closed macular holes postoperatively, respectively. *BCVA with MH without retinal detachment because of no data at the onset of MHRD. This patient initially underwent vitrectomy for MH without retinal detachment in highly myopic eye and she developed MHRD after the initial vitrectomy during hospitalization. We performed vitrectomy with scleral imbrication for her as reoperation. Unfortunately, we did not have her BCVA data at the onset of MHRD after the initial vitrectomy. **B.** The mean changes in the BCVA after scleral imbrication. *$P < 0.05$; **$P < 0.01$.

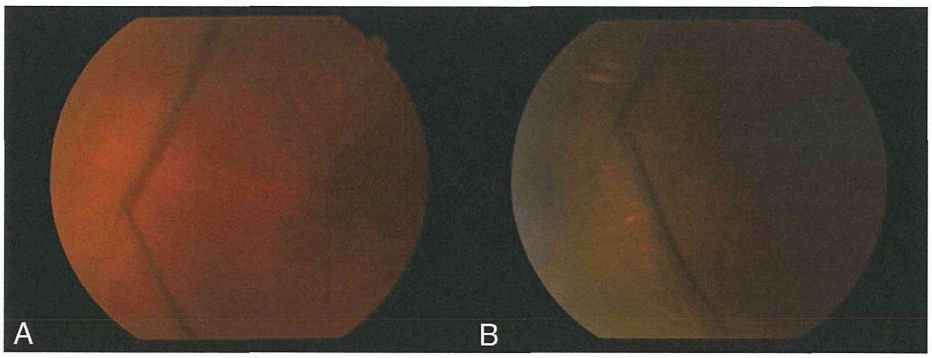

Fig. 2. Color fundus photograph of temporal side in the right eye of the same patient at 6 months (**A**) and 20 months (**B**) after scleral imbrication.

technique for MHRD associated with high myopia have been published. In the two previous studies, the retinal reattachment and closure of MH were assessed based on ophthalmoscopic examination and not OCT during a limited follow-up period. We performed scleral imbrication with PPV and gas tamponade as a second surgery and assessed the efficacy and the anatomical outcome using OCT, especially in eyes with an MHRD considered refractory over the long term.

It was reported that the maximal Snellen visual acuity in MHRD was 20/100 even with MH closure after treatment.[9] In this study, the visual acuity improved in all eyes; in 3 of the 8 eyes, the visual acuity reached a maximum of 0.3 or better using the Landolt chart test postoperatively. This result was favorable for the visual prognosis in MHRD and may be attributable to high rates of reattachment and MH closure achieved with axial length shortening. Not only reattachment but also MH closure should be essential to a better prognosis in MHRD. We observed MH closure in 6 (75%) of the 8 eyes confirmed by spectral domain OCT. Kono et al[18] performed lamellar scleral resection technique combined with PPV, epiretinal membrane peeling, and gas tamponade in 17 eyes with an MHRD and achieved reattachment in all eyes and MH closure in 14 of the 17 eyes (82.4%). This result had a higher rate of MH closure than our result; however, it was assessed ophthalmoscopically, and small MH might have been overlooked. We confirmed the retinal reattachments and closures of MHs based on OCT findings. The visual outcomes may be poor despite retinal reattachment and MH closure.[9] Other factors such as the degree of chorioretinal atrophy may

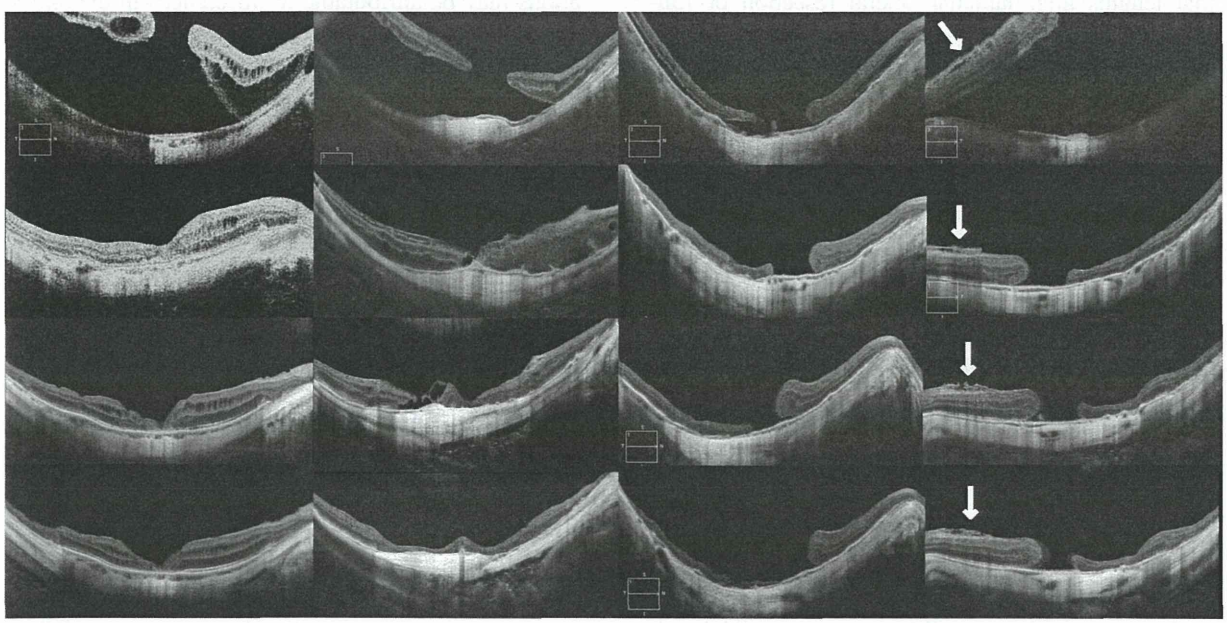

Fig. 3. Optical coherence tomography images in 4 cases including 2 cases with closed MH (2 rows in the left side) and 2 cases with open MH (2 rows in the right side). The lines are before and at 1 month, 12 months, and final visit after scleral imbrication, respectively, beginning at the top. The arrows indicate the residual epiretinal membranes.

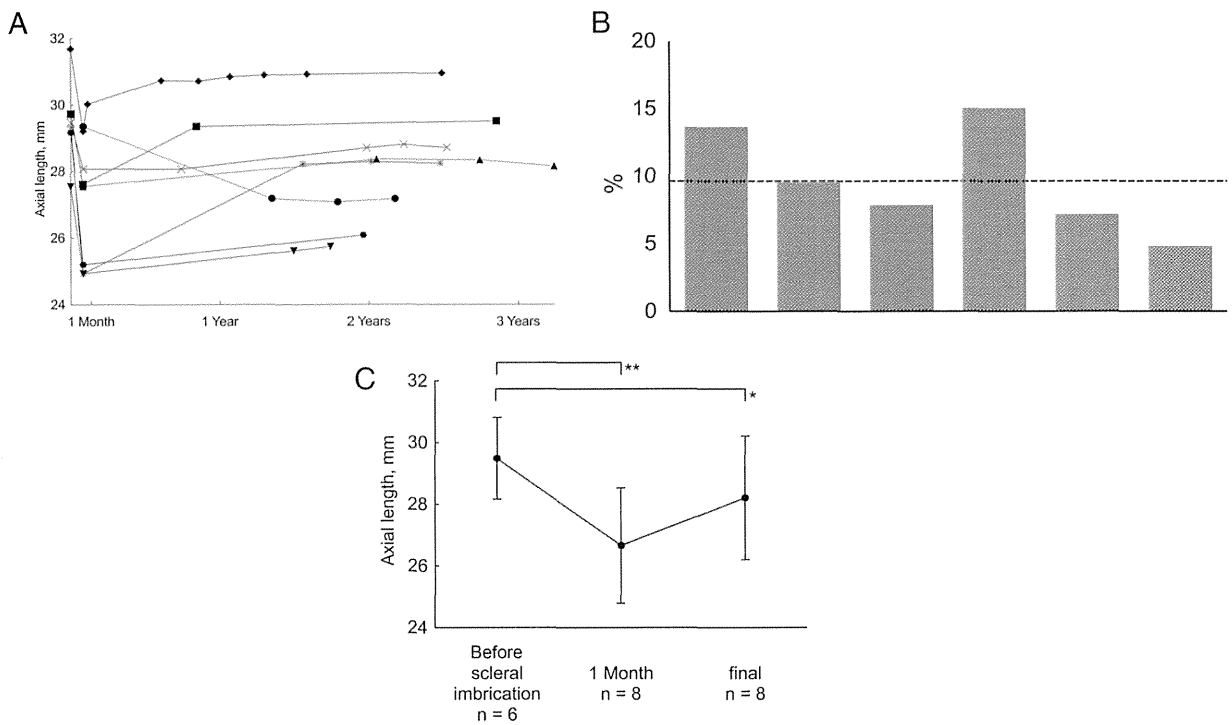

Fig. 4. A. The changes in axial length after scleral imbrication. The dashed lines indicate cases without preoperative data. **B.** The percent decrease in axial length at 1 month after scleral imbrication. The dashed line indicates the mean. **C.** The mean axial length before, 1 month, and at the final visit after scleral imbrication. $*P < 0.05$; $**P < 0.01$.

affect the visual outcomes of retinal detachment surgery in highly myopic eyes.

Nakagawa et al[19] reported the directly measured axial lengths after lamellar scleral resection or full-thickness scleral invagination in enucleated human eyes shortened by approximately 25% of the resection or invagination width and the authors reported a correlation. Based on their report, the mean change in the axial length in this study was estimated to be 2.0 mm and the mean reduction of the axial length 1 month after scleral imbrication was 2.8 ± 1.1 mm in our results. It was longer than that of the report by Matsumura and Ogino,[10] that is, 1.8 mm by the 7.8 ± 2.0-mm width of the lamellar scleral resection. However, our result was shorter than that of Matsuo et al,[13] which was 3.99 mm by 7-mm width of the scleral imbrication. These variations may be attributable to differences in the shortening interval along with individual scleral rigidity and the scleral thickness as reported by Matsuo et al.[13] The difference between lamellar resection and full-thickness imbrication also may affect the postoperative axial length. We think 8.0-mm bite would be safe and enough in this technique, and it should be considered as a second surgery especially in refractory cases. In addition, we evaluated the axial length before and after scleral imbrication with optical coherence biometry.

Table 2. Changes in Millimeters in Axial Length Before, 1 Month, and at the Final Visit After Scleral Imbrication

Case	Before	1 Month	Final Examination	Δ1 Month*	ΔFinal Examination*	Rebound†
1	29.5	28.1	28.7	1.4	0.8	0.6
2	—	27.6	28.2	—	—	0.6
3	27.5	24.9	25.7	2.6	1.8	0.8
4	29.2	25.2	26.1	4.0	3.1	0.9
5	31.7	29.2	31.0	2.5	0.7	1.7
6	29.7	27.6	29.5	2.1	0.2	1.9
7	29.3	24.9	28.2	4.4	1.1	3.3
8	—	29.4	27.2	—	—	−2.2

*Difference from before scleral imbrication.
†Difference between 1 month and at the final visit after scleral imbrication.

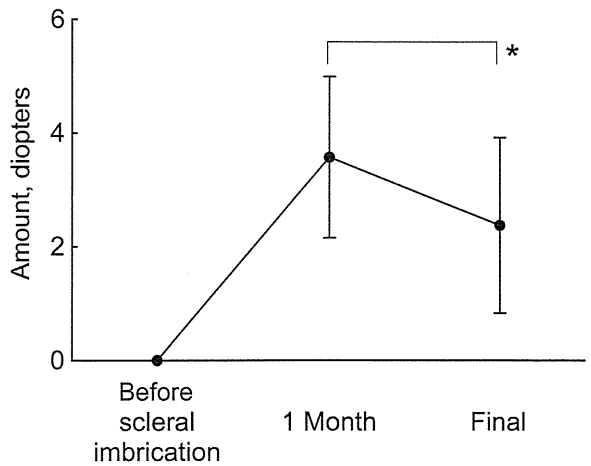

Fig. 5. The mean surgically induced astigmatism at 1 month and the final visit after scleral imbrication. $*P < 0.05$.

We measured several times in each measurement to confirm reproducibility; the measurement was to the level of the retinal pigment epithelium to avoid retinal pathologies such as retinal atrophy or detachment because the conventional ultrasound A-mode scan may have considerable variation especially in case that the patient's fixation is unstable with retinal detachment in the macular area.

Matsumura and Ogino[10] reported against-the-rule astigmatism of 3 to 4 D, and Matsuo et al[13] also reported against-the-rule astigmatism of 4 to 5 D. In this study, we found an average SIA of 3.6 D at 1 month after scleral imbrication, which was comparable with the previous reports. All eyes had regular astigmatism, and six eyes had against-the-rule astigmatism at final visit. This might be acceptable because the postoperative BCVA would be insufficient in most cases with an MHRD and also they could be corrected with cylindrical lenses. This should be considered when intraocular lenses are implanted simultaneously. Implantation of a toric intraocular lens may be an option.

During long-term follow-up, the mean axial length at the final visit remained significantly shorter after scleral imbrication than at baseline and the individual axial length tended to elongate with time, with some cases having considerable elongation during follow-up. However, the axial length remained stable once the change occurred. We calculated the difference between 1 month and the final visit after scleral imbrication and defined that as the rebound (Table 2). The changes in 4 of 8 eyes remained within 1.0 mm, and the axial shortening was considered to be retained to the final visit, and in 3 eyes, the rebound exceeded 1.7 mm at the final visit. In one eye, the axial length shortened further at the final visit presumably because of a measurement error due to posterior staphyloma. However, no correlation was found between the amount of rebound of the axial length and the SIA from 1 month to the final visit after scleral imbrication. Once MHRD has reattached and the posterior eye wall was flattened after scleral imbrication, the flattened convexity of posterior eye wall was sustained to final examination and retinal reattachment. Therefore, those configurations of posterior eye wall may be crucial even after a certain amount of rebound in the axial length. The significant rebound may be occurred not by the laxity of sutures or progress of posterior staphyloma but by the reversion of whole or equatorial eye wall judging by the configurations in fundus photographs and OCT images (Figures 2 and 3).

Of 2 cases without closure of MH, we found thinning of retina with steeper posterior staphyloma in 1 eye and residual epiretinal membrane despite mild convexity of the posterior eye wall in the other eye (the third and fourth row in Figure 3, respectively). These factors may cause failure in MH closure. We also found a slow decline in the BCVA over the long term in some cases. These results suggested continuing spontaneous elongation of the axial length in highly myopic eyes. Saka et al[20] reported that the spontaneous elongation of axial length in highly myopic eyes was 0.08 mm to 0.2 mm annually, especially in elderly patients and eyes with posterior staphyloma. The development of chorioretinal atrophy accompanied by elongation of the axial length could be persistent even after scleral shortening in some highly myopic eyes. However, no eyes in this study developed a retinal redetachment or reopening of a MH during the long-term follow-up period. The amount of mean SIA also decreased significantly between 1 month and the final visit after scleral imbrication, but this was considered to be the natural course.

The current data supported the contention that the scleral imbrication combined with PPV and gas tamponade produced shortening of axial length and flattening of the posterior eye wall including the posterior staphyloma, thus both shortening and flattening may facilitate the retinal reattachment and the closure of MH with the long-term stability in cases with refractory MHRD. Vitrectomy with ILM peeling and gas tamponade may be enough, as an initial surgery considering recent reports.[8,9] However, the scleral imbrication should be considered as a second surgery especially in such refractory cases. Our observations should be confirmed by further investigation because this study was retrospective with a small number of cases.

In conclusion, the scleral imbrication technique combined with PPV can be one option to achieve successful retinal reattachment and MH closure in

patients with refractory MHRD associated with high myopia during long-term follow-up.

Key words: gas tamponade, macular hole, retinal detachment, scleral imbrication.

References

1. Gonvers M, Machemer R. A new approach to treating retinal detachment with macular hole. Am J Ophthalmol 1982;94: 468–472.
2. Blankenship GW, Ibanez-Langlois S. Treatment of myopic macular hole and detachment. Intravitreal gas exchange. Ophthalmology 1987;94:333–336.
3. Ando F. Use of a special macular explant in surgery for retinal detachment with macular hole. Jpn J Ophthalmol 1980;24:29–34.
4. Miyake Y. A simplified method of treating retinal detachment with macular hole. Am J Ophthalmol 1984;97:243–245.
5. Sasoh M, Yoshida S, Ito Y, et al. Macular buckling for retinal detachment due to macular hole in highly myopic eyes with posterior staphyloma. Retina 2000;20:445–449.
6. Spaide RF. Measurement of the posterior precortical vitreous pocket in fellow eyes with posterior vitreous detachment and macular holes. Retina 2003;23:481–485.
7. Ripandelli G, Parisi V, Friberg TR, et al. Retinal detachment associated with macular hole in high myopia: using the vitreous anatomy to optimize the surgical approach. Ophthalmology 2004;111:726–731.
8. Ortisi E, Avitabile T, Bonfiglio V. Surgical management of retinal detachment because of macular hole in highly myopic eyes. Retina 2012;32:1704–1718.
9. Ryan EH Jr, Bramante CT, Mittra RA, et al. Management of rhegmatogenous retinal detachment with coexistent macular hole in the era of internal limiting membrane peeling. Am Journal Ophthalmol 2011;152:815–819. e811.
10. Matsumura M, Ogino N. A surgical approach for macular hole retinal detachment associated with high myopia. Jpn J Ophthalmic Surg 1996;9:425–428.
11. Shimizu E, Ohta T, Kogishi J. Scleral resection for retinal detachment with macular hole after failure of intraocular gas. Jpn Rev Clin Ophthalmol 1994;88:1583–1586.
12. Ueda T, Kogishi J, Matsumura M, et al. Therapeutic approach in retinal detachment with macular hole after failure by intraocular gas and laser photocoagulation. Jpn Rev Clin Ophthalmol 1992;86:2616–2620.
13. Matsuo T, Shiraga F, Takasu I, Okanouchi T. Scleral infolding combined with vitrectomy and gas tamponade for retinal detachment with macular holes in highly myopic eyes. Jpn J Ophthalmol 2001;45:403–408.
14. Holladay JT. Proper method for calculating average visual acuity. J Refract Surg 1997;13:388–391.
15. Chamlin M, Rubner K. Lamellar undermining; a preliminary report on a technique of scleral buckling for retinal detachment. Am J Ophthalmol 1956;41:633–638.
16. Mikuni M, Kobayashi S, Yaoeda H. Treatment of retinal detachment with macular hole [in Japanese]. Nihon Ganka Kiyo 1967;18:659–668.
17. Amemiya T, Iida T. Results and complications of surgery of retinal detachment with a macular hole. Ophthalmologica 1980;181:88–92.
18. Kono T, Takesue Y, Shiga S. Scleral resection technique combined with vitrectomy for a macular hole retinal detachment in highly myopic eyes. Ophthalmologica 2006;220: 159–163.
19. Nakagawa N, Parel JM, Murray TG, Oshima K. Effect of scleral shortening on axial length. Arch Ophthalmol 2000; 118:965–968.
20. Saka N, Ohno-Matsui K, Shimada N, et al. Long-term changes in axial length in adult eyes with pathologic myopia. Am J Ophthalmol 2010;150:562–568 e561.

Original Paper

Ophthalmic Research

Ophthalmic Res 2014;52:234–238
DOI: 10.1159/000365253

Received: February 6, 2014
Accepted after revision: June 14, 2014
Published online: November 14, 2014

Anterior Chamber Paracentesis Might Prevent Sustained Intraocular Pressure Elevation after Intravitreal Injections of Ranibizumab for Age-Related Macular Degeneration

Yusuke Ichiyama Tomoko Sawada Masashi Kakinoki Osamu Sawada
Tomoko Nakashima Yoshitsugu Saishin Hajime Kawamura Masahito Ohji

Department of Ophthalmology, Shiga University of Medical Science, Otsu, Japan

Key Words
Age-related macular degeneration · Intraocular pressure · Ranibizumab · Anterior chamber paracentesis

Abstract
Background/Aims: To evaluate the efficacy of anterior chamber paracentesis for preventing sustained intraocular pressure (IOP) elevation after intravitreal ranibizumab (IVR) injections for age-related macular degeneration (AMD). ***Methods:*** The medical records for all cases of exudative AMD treated with IVR injections and followed monthly for 12 months or longer were reviewed retrospectively. Anterior chamber paracentesis was performed just before IVR injections. A sustained IOP elevation was defined as 22 mm Hg or higher during 2 consecutive visits with an increase exceeding 6 mm Hg from baseline. ***Results:*** One hundred and eleven eyes met the inclusion criteria, and none of these eyes had a sustained IOP elevation. ***Conclusions:*** Anterior chamber paracentesis before IVR injections may prevent sustained IOP elevations.

Introduction

Intravitreal anti-vascular endothelial growth factor (VEGF) agents are used widely to treat neovascular age-related macular degeneration (AMD). Ranibizumab (Lucentis, Genentech, South San Francisco, Calif., USA) [1, 2], pegaptanib sodium (Macugen, Eyetech-OSI, New York, N.Y., USA) [3] and aflibercept (Eylea, Regeneron, Tarrytown, N.Y., USA) [4] have been approved by the US Food and Drug Administration for use in AMD. Bevacizumab (Avastin, Genentech, South San Francisco, Calif., USA), which received initial US Food and Drug Administration approval for use in colorectal cancer [5], is also commonly used as an off-label treatment for AMD. With widespread use of anti-VEGF agents, some studies reported the occurrence of sustained intraocular pressure (IOP) elevation after intravitreal anti-VEGF injections [6–15]. Presently, sustained IOP elevation due to intravitreal injection of anti-VEGF agents is a real concern. Some possible mechanisms underlying sustained IOP elevation after intravitreal injections of anti-VEGF agents have been previously proposed [6–15]. One of them is that the IOP spikes after injection cause damage to the outflow system and in turn prolong IOP elevation [7–11]. To prevent this occurrence, we performed anterior chamber paracentesis just before intravitreal ranibizumab (IVR) injection.

KARGER

E-Mail karger@karger.com
www.karger.com/ore

0030–3747/14/0524–0234$39.50/0

Tomoko Sawada, MD
Department of Ophthalmology
Shiga University of Medical Science
Seta Tsukinowacho, Otsu, Shiga, 520-2192 (Japan)
E-Mail tsawada@belle.shiga-med.ac.jp

The purpose of the current study was to evaluate the efficacy of anterior chamber paracentesis to prevent sustained IOP elevation after IVR injection for AMD.

Materials and Methods

The medical records of patients with AMD treated with IVR injections at Shiga University of Medical Science Hospital from April 2009 to June 2012 were reviewed retrospectively. Patients treated with at least 3 initial IVR injections for exudative AMD with choroidal neovascularization and followed monthly for 12 months or longer were included in this study. Patients treated with antiglaucoma eyedrops were not excluded. The exclusion criteria were treatment with photodynamic therapy combined with IVR injections, vitrectomy with silicone tamponade before the first IVR injection or vitrectomy during the follow-up period. Patients who underwent vitrectomy without silicone tamponade before the first IVR injection were not excluded.

The treatment regimen included 3 consecutive monthly IVR injections followed by a pro re nata dosing protocol. Re-injections were administered with the consent of the patients, if one of the following changes was observed at each visit: a visual acuity loss that exceeded 0.1 logarithm of the minimum angle of resolution (logMAR) unit, recurrent central macular edema or subretinal fluid on optical coherence tomography images (Cirrus HD-OCT, Carl Zeiss Meditec Inc., Dublin, Calif., USA), and new hemorrhages [16].

Each patient provided informed consent before treatment. Four ophthalmologists performed the injections in the office or the operating room using an aseptic technique that included instillation of topical 4% lidocaine hydrochloride and 1.25% povidone iodine, placement of a sterile eyelid speculum, and use of a 30-gauge needle on a 1-ml plastic syringe. The injections were administered using a superior or inferior temporal approach 3.5–4.0 mm from the limbus. All syringes were coated with silicone oil on the syringe barrel and rubber stopper (1-ml tuberculin syringe, Terumo, Tokyo, Japan). An anterior chamber paracentesis was performed just before the IVR injections in all eyes. Anterior chamber paracentesis was performed using a 1-ml plastic syringe with a 29-gauge needle (1-ml Terumo Myjector 29-gauge insulin syringe, Terumo) and obtained 0.1–0.2 ml of aqueous humor. Performance of an anterior chamber paracentesis before IVR injection was approved by the Institutional Review Board of Shiga University of Medical Science. The best-corrected visual acuity was measured using a Landolt C visual acuity chart and was converted to logMAR units for analysis.

The IOP was measured 3 times with a noncontact tonometer (NT-4000 Non-Contact Tonometer, Nidek, Aichi, Japan) and the mean measurement was recorded before and at every follow-up visit after the first IVR injection. A sustained IOP elevation was defined as 22 mm Hg or higher during 2 consecutive visits with an increase from baseline of greater than 6 mm Hg. This definition was based on previous reports [12, 13]. A transient IOP elevation was defined as an increase of greater than 6 mm Hg from baseline, but lasting less than 30 days without the need for medical or surgical treatment. This definition was based on a previous report indicating that normal fluctuation of IOP was usually less than this value [17]. In patients who received IVR injections into 1 eye, the fellow untreated eyes served as controls. Glaucomatous eyes were also evaluated separately.

Table 1. Baseline patient characteristics

Factors	All eyes	Glaucomatous eyes
Number of eyes	111 (100)	9 (8.1)
Number of men	78 (71.6)	5 (55.6)
Age, years		
Mean ± SD	73.0±8.2	77.9±8.0
Range	54–91	65–86
Mean IOP, mm Hg		
Mean ± SD	12.9±3.1	13.0±4.4
Range	7.0–20.3	7.0–20.3

Figures in parentheses are percentages. SD = Standard deviation.

Statistical Analysis

Data were analyzed using Sigma Stat statistical software (version 3.1, Systat Software Inc., Richmond, Calif., USA). The IOP in the injected eyes was compared monthly with the baseline value using the Bonferroni multicomparison test. The total number of injections in eyes with transient IOP elevation was compared with that in eyes without transient IOP elevation using the Mann-Whitney test. Because the number of patients was small, the paired t test was used every month to compare IOP values of glaucomatous, injected eyes with their baseline IOP values. The unpaired t test was used every month to compare the IOP values of the injected eyes with that of their fellow control eyes. $p < 0.05$ was considered significant.

Results

A total of 111 eyes of 109 patients (71.6% men) met the inclusion criteria. The mean patient age at the start of treatment was 73.0 ± 8.2 years. The mean baseline IOP of all injected eyes was 12.9 ± 3.1 mm Hg (table 1). The mean follow-up time was 18.7 ± 4.6 months (range, 12–24). The mean number of injections (including the first 3) was 4.4 ± 1.4 during the first 12 months and 6.0 ± 3.1 during the follow-up period.

No sustained IOP elevation occurred in any eyes throughout the follow-up period (table 2). Transient IOP elevations were found in 4 eyes of 111. One of them received 14 IVR injections, another eye received 7 IVR injections, and the other 2 eyes received 3 IVR injections during the follow-up period. The mean number of IVR injections in eyes with transient IOP elevations did not significantly differ from the mean number of IVR injections in eyes without transient IOP elevations (6.8 ± 5.2 vs. 6.0 ± 1.0, respectively; $p = 0.96$; table 3).

The highest mean IOP during the follow-up period was 12.9 ± 3.0 mm Hg at month 21, which did not differ significantly ($p = 1.0$) from the mean baseline IOP (fig. 1).

Table 2. Postinjection data from all eyes and glaucomatous eyes receiving ranibizumab

Factors	All eyes (n = 111)	Glaucomatous eyes (n = 9)
Sustained IOP elevations, n	0 (0)	0 (0)
Transient IOP elevations, n	4 (3.6)	1 (11.1)
Follow-up, months		
Mean ± SD	18.7±4.6	19.4±5.1
Range	12–24	12–24
Number of injections		
Mean ± SD	6.0±3.1	7.4±4.6
Range	3–14	3–14

Figures in parentheses are percentages. SD = Standard deviation.

Table 3. Postinjection data from all eyes and eyes with or without transient IOP elevation

Factors	All eyes	Eyes with transient IOP elevation	Eyes without transient IOP elevation	p value
Number of eyes	111 (100)	4 (3.6)	107 (96.4)	
Mean number of injections ± SD	6.0±3.1	6.8±5.2	6.0±3.0	0.96

Figures in parentheses are percentages. SD = Standard deviation.

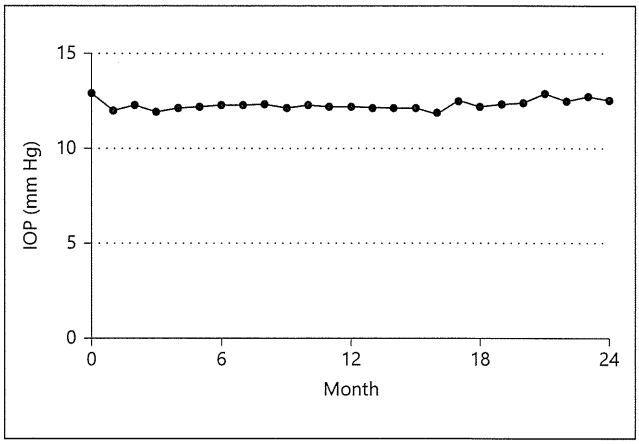

Fig. 1. The mean monthly IOP values in all study patients. The highest mean IOP during the follow-up period is 12.9 ± 3.0 mm Hg at month 21, which does not differ significantly compared with the mean baseline IOP.

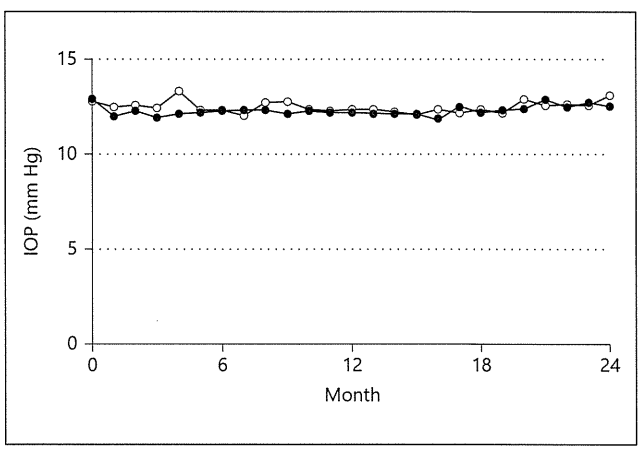

Fig. 2. The mean monthly IOP values in the eyes injected with IVR (closed circles) and the fellow eyes (open circles). The highest mean IOP of the injected eyes during the follow-up period is 13.1 ± 2.9 mm Hg at month 21, which does not differ significantly from the mean baseline IOP. There is no significant difference in the mean IOP between the treated eyes and the control fellow eyes.

One hundred and seven patients were treated in 1 eye, but the IOP of the fellow eye was not measured in one of these patients because of severe corneal opacity and the onset of phthisis bulbi. Therefore, we compared the mean IOP between the treated eyes and the fellow control eyes in 106 patients. The highest mean IOP of the injected eyes during the follow-up period was 13.1 ± 2.9 mm Hg at month 21, which did not differ significantly from the mean baseline IOP (p = 1.0). There was no significant difference in the mean IOPs between the treated eyes and the fellow control eyes (fig. 2).

Nine eyes of 9 patients, at baseline, had both AMD and glaucoma [normal tension glaucoma (4 eyes), primary open-angle glaucoma (4 eyes) and pseudoexfoliation glaucoma (1 eye)]. All eyes were treated with glaucoma eyedrops. All patients with AMD and glaucoma received IVR injections in 1 eye. The mean baseline IOP was 13.0 ± 4.4 mm Hg, and the highest mean IOP during the follow-up period was 13.0 ± 4.0 mm Hg at month 23, which did not differ significantly from the mean baseline IOP (p = 0.88). No patient had concomitant initiation or augmentation of IOP-lowering therapy with development of glaucomatous visual field loss. There was no significant difference in the mean IOP between the treated eyes and control eyes during the follow-up period in the patients with AMD and glaucoma (fig. 3).